2019 International Conference on Robotics and Automation (ICRA)
Palais des congres de Montreal, Montreal, Canada, May 20-24, 2019

Optical Force Sensing In Minimally Invasive Robotic Surgery

Amir Hossein Hadi Hosseinabadi, Mohammad Honarvar, Septimiu E. Salcudean, *Fellow, IEEE*

***Abstract*— This paper evaluates the feasibility of a novel optical sensing concept to measure forces applied at the tip of daVinci EndoWrist instruments. An optical slit is clamped onto the instrument shaft, in-line with an infrared LED-bicell pair. Deflection of the shaft moves the slit with respect to the LED-bicell pair and modulates the light incident on each active element of the bicell. The differential photocurrent is conditioned and monitored to estimate the tip forces. The feasibility evaluation consists of a flexible beam model to quantify the required sensor performance, experimental results with a 3D printed prototype and estimation of the sensor limitations including the measurement bandwidth due to the structural dynamics. The proposed approach requires no modifications to the instrument, is adaptable to different instruments and robot platforms, and leads to high-resolution, high-dynamic range sensing without hysteresis.**

***Keywords*— Surgical Robotics: Laparoscopy, Force and Tactile Sensing, Haptics and Haptic Interfaces**

I. Introduction

A. Motivation

Despite the growing popularity of Robot-Assisted Minimally Invasive Surgery (RAMIS) over the past decade [1], no surgical robot currently in clinical use provides force feedback to the surgeon [2]. This deprives the surgeon of the rich information embedded in palpating the tissue and in the direct interaction with surgical tools. To provide accurate force feedback to the operator in normal use, and even to evaluate whether haptic feedback is useful in experimental systems, instrument forces must be measured during surgery [3]. Apart from haptic feedback, measuring instrument-tissue interaction forces has many applications, including monitoring tissue damage, developing training guidelines for robotic surgery, and determining the expertise of surgeons.

Model-based force estimation is possible by using a Kalman filter [4] or a disturbance observer [5], [6]. However, the accuracy of these methods is limited by the accuracy of the model that can vary with the life of the tool [7]. According to previous studies [8], [9], the most important forces of interaction that should be measured in surgical applications are 1) lateral forces, 2) axial forces and 3) the axial torque about the instrument's shaft, in the presented order. The measurement of instrument-tissue forces remains a major challenge that has intrigued many researchers in the field of sensor design. This is due to the size, sterilizability, biocompatibility, and cost considerations of RAMIS instruments.

B. Background and Research Objective

The focus in our research is on developing a force sensor to primarily measure the lateral forces applied at the tip of RAMIS instruments with 0.2 (N) accuracy over a range of ±10 (N) as suggested in [3]. Estimation of the axial force and the torque about the instrument shaft is a secondary objective [8], [9]. However, to the best of our knowledge, no performance requirement in these two degrees of freedom is specified in the literature. The force sensor is required to be adaptable to different daVinci EndoWrist instruments with no modification needed in the instrument structure.

Conventionally, strain gauges have been used to estimate the tip-forces from strains developed within the instrument shaft. Strain gauges were installed at the instrument base [10], instrument shaft [9], [11], [12], trocar [13], the instrument cables [14], the articulated joint [15], [16], the instrument grippers [17], the and different combinations of the above [18]–[20] to estimate the instrument tip forces. The closer the sensor is placed to the instrument tip, the more accurate the force estimation will be; however, the design constraints will be more stringent. These transducers require modifications to the instrument to amplify local strains. They also need special surface preparation, adhesives and coatings to achieve optimal performance and to survive the sterilization process [21].

Kim et al. [22] designed forceps with integrated capacitive force sensors to estimate the 3-DOF forces as well as the gripping force. Piezoelectric [23], pneumatic [24], and MEM [25] techniques are also presented in the literature for design of tactile and force sensors in RAMIS and MIS (Minimally Invasive Surgery) applications.

There is ample literature on the use of optical techniques in force sensor design where light modulation is used for force measurement. The light modulation can happen by an external component (e.g. a reflective surface) or within an optical element (e.g. Fiber Brag Gratings - FBG). The modulated light can be locally converted to an electric signal (e.g. photodiodes) or be transferred through a transduction element (e.g. optical fibre) for distal processing.

Lazermos et al. [26] proposed the integration of optical fibers in the design of forceps. Peirs et al. [27] designed a special flexure with integrated micro fibers for 3-DOF force estimation in laparoscopic instruments. Muller et al. [28] and Haslinger et al. [29] integrated FBGs in a Stewart platform sensor design proposed by Seibold et al. [15]. In [30] by Song et al., four FBGs were embedded in the distal shaft of the instrument, inside the abdominal cavity. Puangmali et al. [31] proposed a design similar to [27] which is based on reflective light intensity modulation for a palpation application.

A.H. Hadi Hosseinabadi (ahhadi@ece.ubc.ca), M. Honarvar (honarvar@ece.ubc.ca) , and S. E. Salcudean (tims@ece.ubc.ca) are with the Robotics and Control Laboratory, Department of Electrical and Computer Engineering, University of British Columbia, Vancouver, BC V6T 1Z4, Canada.

Shahzada [2] installed four FBGs in a two cross-section design on the distal shaft of a daVinci instrument. As can be inferred from the cited literature, FBGs are becoming a popular alternative for force sensing in medical applications due to their high sensitivity and signal-to-noise ratio, small size, biocompatibility, sterilizability and EM isolation [2].

All of the approaches reported above require modifications of the instrument or the robot to integrate the force sensor. In recent work, Fontanelli et al. [32] placed four optical proximity sensors at the trocar to measure the lateral forces applied at the instrument tip. The proposed design required no modification of the tool and is therefore adaptable to different RAMIS instruments. The sensor needs to be placed within the abdominal cavity and the size of the access hole has to be larger than the trocar itself to accommodate the sensor. Moreover, the straightness and circular run-out of the instrument shaft along its length must be compensated for.

Figure 1. Optical sensor + low friction trocar and a compliant interface to the instrument

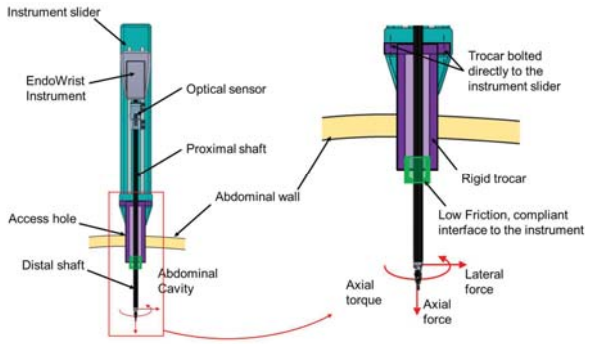

Due to stringent constraints on the sensors that enter the abdominal cavity, we researched a solution to be installed onto the proximal shaft. While this approach benefits from the more relaxed design constraints, the sensor readings will be affected by the friction forces at the trocar, the interaction forces with the abdominal wall, the forces from nearby organs [3], and the instrument dynamics between the force actuation and measurement points. The small gap between the instrument shaft and the trocar's inner hole causes changes in the support boundary conditions of the instrument shaft when it bends. This can cause a dead-band, which changes with instrument insertion depth, over which a linear calibration would not work [20]. A rigid, low friction trocar with a compliant interface to the instrument (Fig. 1) can resolve this; the forces from the abdominal wall are transferred to the instrument slider through the rigid trocar. This is similar to the overcoat concept presented by Shimachi et al. [19]. The low friction interface between the instrument and the trocar minimizes the effect of friction forces. The stiffness of the compliant interface to the instrument could be adjusted to avoid hitting the trocar (closing the gap) at the maximum force (±10 (N)). Therefore, our research objective, at a high level, is developing a sensor to estimate the instrument tip forces from the deflections at the proximal shaft of the daVinci EndoWrist instruments which pass through a rigid, low friction trocar with a compliant interface. Design of the modified trocar is part of the future work and is not the focus in this paper.

Looking for simplicity, versatility, and a cost-effective solution, we were inspired by the bending displacement sensor proposed by Barret and Quate [33] for optical scan-correction in Atomic Force Microscopy (AFM). The reported performance metrics make it a promising candidate to replace strain gauges and detect very small deflections at the proximal instrument shaft. As shown in Fig. 2, the proposed sensor is comprised of an Infrared (IR) Light Emitting Diode (LED) placed in-line with a bicell photodetector, and an optical slit to modulate the light received by each cell. The differential bicell photocurrent could be monitored to detect the displacement of the optical slit with respect to the LED-bicell pair.

Figure 2. Optical sensor to detect the displacement of the optical slit w.r.t the LED-bicell pair

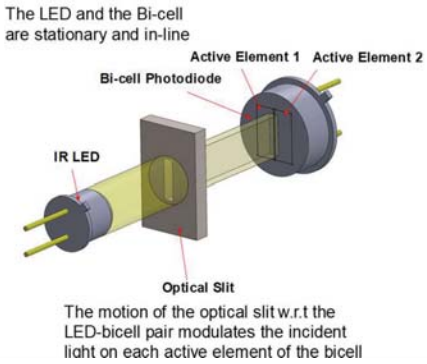

C. *Scope of Work and Paper Structure*

Within our research objective, this work evaluates the feasibility of using the sensing scheme above to estimate the lateral forces applied at the instrument tip. Successful force estimation based on the bicell readings justifies further research and design work toward expanding the presented concept to other degrees of freedom and design of a compliant, low-friction trocar. A force sensor design with bicells will be inexpensive, easy to install, and highly adaptable with no modification required to the EndoWrist instruments design.

Section II explains the test setup used for the feasibility evaluation. In Section III, the sensor performance requirement is quantified by using a flexible beam model. Section IV elaborates on the sensor calibration and the results. A lower bound on the accuracy of the sensor readings is calculated in Section V. Section VI concludes this paper and briefly comments on the future work.

II. TEST SETUP

The assembly shown in Fig. 3 was used to evaluate the feasibility of using the sensing scheme explained above to estimate the lateral forces applied at the instrument tip. In this setup, an IR LED and a bicell photodiode where concentrically mounted onto the instrument shaft, 15 (mm) away from the base of the instrument. A 2 (mm) thick aluminum plate with a slit of 1 (mm) wide was mounted on the instrument shaft such that the IR light beam passes through the slit and impinges upon the bicell. The holder of the LED and the bicell, and the holder of the aluminum slit were 3D printed in PLA. The holders were clamped on the instrument shaft 35 (mm) apart. The deflection of the instrument shaft leads to a displacement of the aluminum slit with respect to the LED-bicell pair and

consequently change in the light received by each active element of the bicell.

Figure 3. Single axis bicell sensor

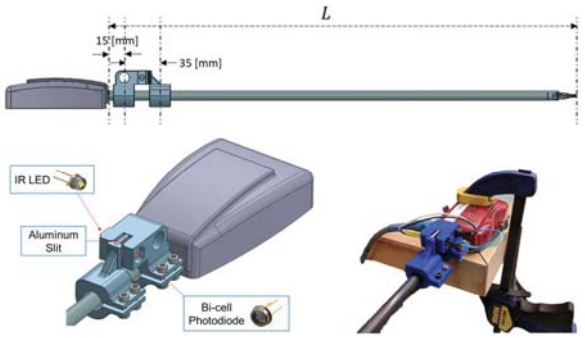

The differential photocurrent of the active elements was converted to a voltage through a signal conditioning circuitry shown in Fig. 4. It is comprised of two Trans-impedance Amplifiers (TA) to convert the photocurrent into voltage and a high precision differential Instrumentation Amplifier (IA). The differential signal was fed through a low pass filter with the cut-off frequency of ~500 (Hz) before being amplified. In order to null the output voltage (V_{IA}) at no load, an offset voltage (V_{OS}) is applied before the trans-impedance circuit to add to/subtract from the photocurrent out of one of the cells. While the electronics for this application is fairly conventional, the nulling of the sensor readings at the photocurrent level (before being amplified by TAs) had not been reported before. This nulling approach allows for a large offset adjustment range and eliminates the need for tight control on installation tolerances.

Figure 4. Electronics schematics for the bicell sensor

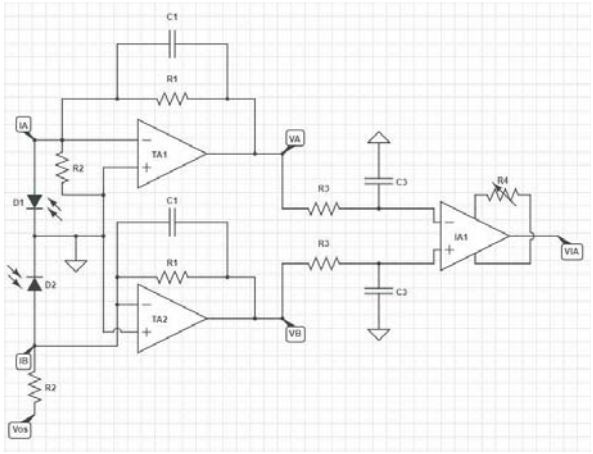

III. Instrument Model as a Flexible Beam

A bending model of the flexible surgical instrument when interacting with tissues inside a patient and the trocar at the input port was presented in [34]. The instrument is made of a carbon fiber tube in which 6 pre-tensioned hollow steel wires are located to drive the instrument's wrist (Fig. 6). Due to the symmetric cross-section, the *y*- and *z*-axis are also the neutral axes of the composite cross-section. Without the trocar, the bending behavior of the EndoWrist instruments could be modeled as a clamped beam, shown in Fig. 5, with the deflection curve of the beam expressed as [35]:

$$y = \frac{F}{EI_{zz}}\left(\frac{x^3}{3} + \frac{(L-x)x^2}{2}\right),\ 0 \le x \le L \qquad (1)$$

where F is the lateral force applied at the tip of the instrument, E = 150 (GPa) is the Young's modulus for carbon fiber, L = 420 (mm) is the length of the instrument, and I_{zz}=152.7 (mm^4) is the total moment of inertia of the composite cross-section of the beam about its z-neutral axis. A similar equation exists for the bending profile in the z direction with I_{yy}=131.75 (mm^4). Excluding the steel wires from the calculations leads to 20% and 3% increase in the estimated deflections in the y- and z-directions, respectively.

Figure 5. Instrument modeled as a clamped flexible beam

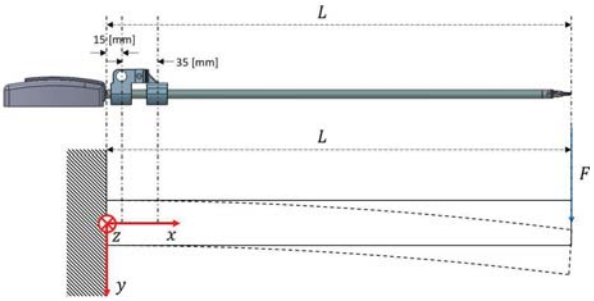

The beam deflection profiles in the lateral directions, for 1 (N) force applied at the instrument tip, are depicted in Fig. 7. As the plots show (red: y and blue: z), when the maximum deflection at the instrument tip is ~1.2 (mm), the relative deflection between the slit center and the LED-bicell center is approximately 25 (µm).

Figure 6. Composite cross-section of the instrument

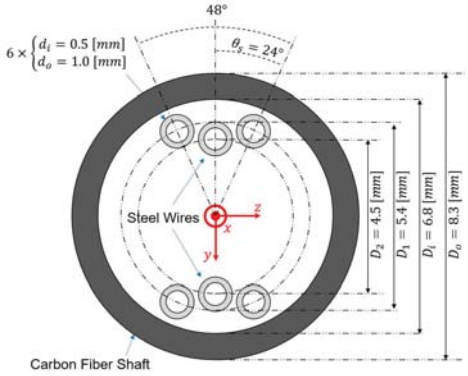

The current model does not include the trocar complexities that were explained in Section I. As expressed earlier, the end goal is achieving 0.2 (N) accuracy over ±10 (N). Allowing for the same maximum deflection in the final sensor design with the modified trocar (Fig. 1), the bicell sensor should measure deformations of up to ±25 (µm) with accuracy of $\frac{0.2(\text{N})}{10\ (\text{N})} \times 25\ (\mu\text{m}) = 0.5\ (\mu\text{m})$ or better. Decreasing the maximum allowable deflection (e.g. from 1.2 (mm) to 0.5 (mm) or smaller) linearly decreases the accurate deflection detection threshold (e.g. from 0.5 (µm) to 0.2 (µm) or smaller). The sensor performance is further analyzed in Section V.

Figure 7. Deflection profile of the instrument in the lateral (y and z) directions

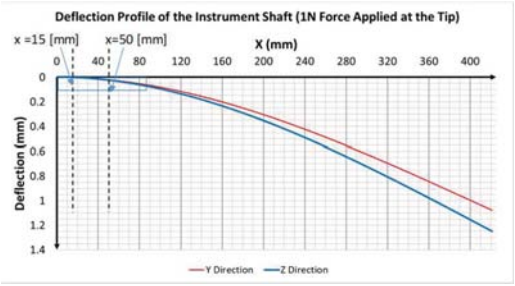

(a) Deflection profiles over the full length of the instrument

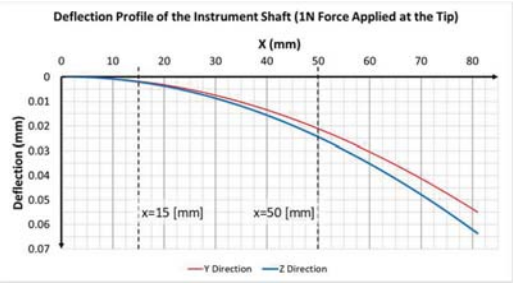

(b) Deflection profiles over the blue box in Figure (a)

IV. Sensor Calibration

To calibrate the sensor readings, a six-axis force sensor (ATI Nano17) was mounted at the tip of the instrument as shown in Fig. 8. The optical sensor and ATI readings were nulled after installation of the ATI force sensor to zero out all the readings before starting the calibration.

Figure 8. Calibration setup

Fig. 9 depicts the time-history calibration data for the optical sensor where a cyclic force is applied in the y direction to the ATI force sensor at the tip of the instrument. The plot shows a delay between the bicell sensor output (V_{IA}) and readings of the ATI force sensor in y direction (F_{ATIy}); this was expected, as the data logging was not synchronized.

Figure 9. Instrument modeled as a clamped flexible beam

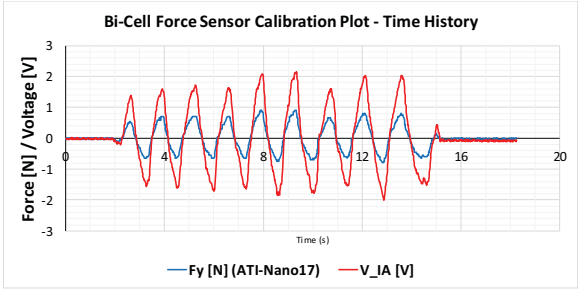

The equation below was used for sensor calibration:

$$F_{ATI}(k) = a_0 V_{IA}(k - a_1) + a_2 \quad (2)$$

where a_0 is the calibration constant (N/V) , a_1 is the delay in sample numbers (dmls), and a_2 is the dc offset between the two readings (N). a_1 is identified by maximizing the normalized cross-correlation between the two readings. As plotted in Fig. 10, the cross-correlation is maximum when the lag between the two readings is 5 ($a_1 = 5$).

Figure 10. Normalized cross correlation plot between F_{ATI} and V_{IA}

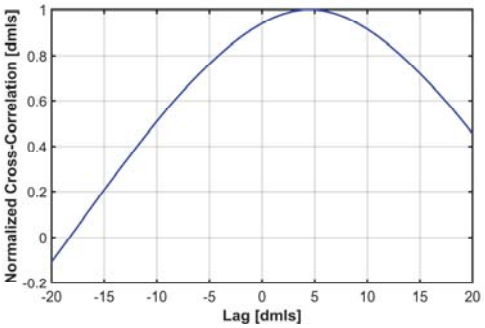

a_0 and a_2 are identified by reformulating the calibration equation (2) in matrix form (3) and using the least squares technique (4).

$$F_{ATI}(k) = \underbrace{[V(k - a_1) \quad 1]}_{X(k,:)} w \text{ where } w = \begin{bmatrix} a_0 \\ a_2 \end{bmatrix} \quad (3)$$

$$w = \underset{w}{argmin} \, ||F_{ATI} - Xw||_2^2 = (X^T X)^{-1} X^T F_{ATI} \quad (4)$$

Figure 11. Bicell sensor calibration plot a_0=0.4137 (N/V), a_2= 0.0024 (N)

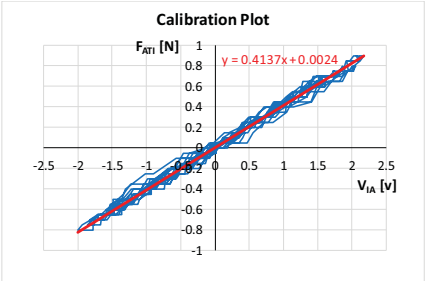

Fig. 11 shows the calibration plot and the identified a_0 = 0.4137 (N/V) and a_2 = 0.0024 (N). As the calibration plot shows, the bicells response is linear with no hysteresis behavior. In this experiment, the gain of the instrumentation amplifier was set to 133 which resulted in a peak voltage of ~ 2 (V) due to the corresponding *relative* displacement of the aluminum slit at the sensor location when a lateral force of ~ 0.8 (N) is applied at the instrument tip.

It is important to note that the bending dynamics of the instrument shaft is between the force actuation point and where the bicell sensor is mounted. In order to identify the frequency range over which the calibration above is valid, the impulse response of the instrument shaft (as shown in Fig. 12(a)) was captured. The impulse response was further processed in MATLAB to quantify the instrument shaft

dynamics; as Fig. 12(b) shows, its damped frequency, $F_d = F_n\sqrt{1-\zeta^2} = 24$ (Hz), where F_n is the natural frequency and ζ is the damping ratio of the instrument bending dynamics. The power constant of the exponential fit to the impulse response peaks is equal to $-2\pi\zeta F_n$ [36]. Considering the average of power constants of the exponential term in the positive and negative fits, $-2\pi\zeta F_n = -4.83$. Solving the two equations above results in the followings:

$$\zeta = 0.032 \text{ (dmls)}, F_n = 24.012 \text{ (Hz)}. \quad (5)$$

Figure 12. Impulse excitation of the instrument shaft in the lateral direction

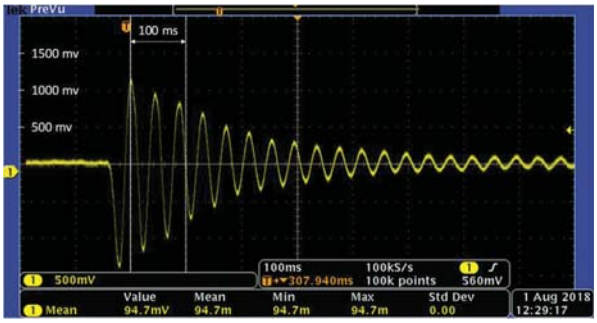

(a) V_{IA} readings in the Oscilloscope - Tektronix MSO 3014

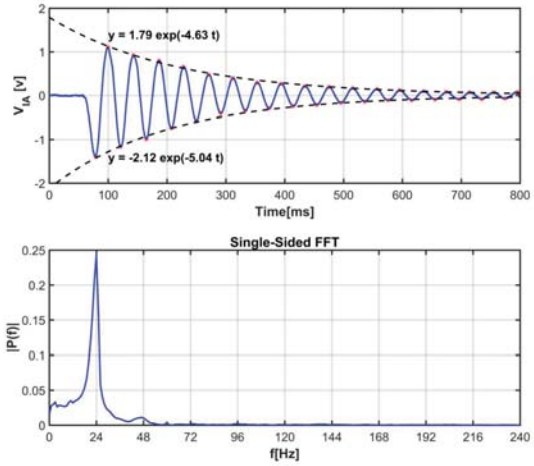

(b) Processed data to identify the modal parameters

The transfer function of the instrument shaft bending from the applied force at the instrument tip (F_y) to the bicell voltage outputs (V_{IA}) can be represented as a single degree of freedom system given in (6) below:

$$\frac{V_{IA}}{F_y} = \frac{a_3}{s^2+2\zeta\omega_n s+\omega_n^2} \quad (6)$$

where:

- $\omega_n = 2\pi F_n$
- $\frac{a_3}{\omega_n^2} = \frac{1}{a_0}$ and a_0 was identified in the previous section as 0.4137 (N/V)

Hence, a_3 = 5502.3 (V/N.s^2). The Bode plot of the instrument bending dynamics (6) is shown in Fig. 13. Considering ±3 (dB) offset from the dc value, the bandwidth of the sensor measurements, over which the calibration above is valid, is ~13 (Hz). The dynamic response of the instrument, and therefore the reported measurement bandwidth change with adding the trocar and the instrument insertion.

Figure 13. Bode plot of the instrument's bending dynamics

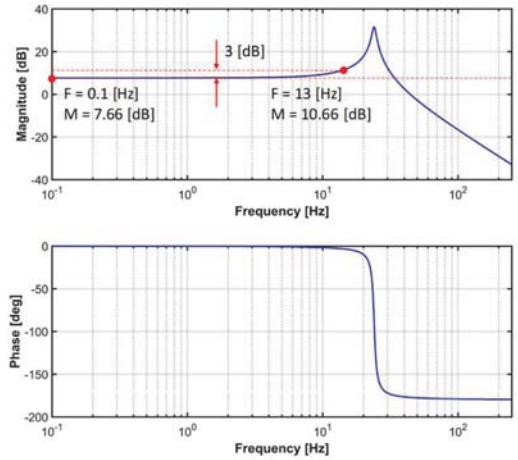

The first two plots in Fig. 14 compare the resolved force data calculated by using the identified calibration equation (2) with the ATI force sensor readings in y direction. The plots show good tracking of the force readings with a standard deviation of the error signal of 0.032 (N). The followings contribute to the presented tracking error:

- The resolution of the ATI force sensor is limited to 0.05 (N)
- High frequency dynamics (beyond 13 (Hz)) at the peaks.
- Cross-talk in the z direction during calibration as the third plot shows. While a single-axis calibration sees this as calibration inaccuracy, a multi-axis calibration scheme, in which another optical transducer is added in the z direction, would take the cross-talk into account and improve the calibration and force estimation accuracy.

Figure 14. Comparison of the ATI force sensor measurements and the bicell sensor measurements

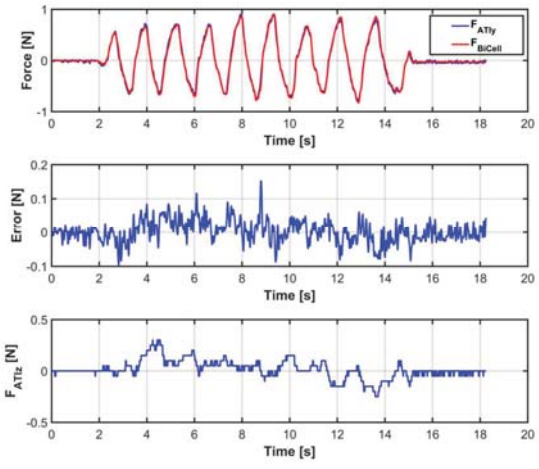

V. Sensor Performance Analysis

From the flexible beam model in Section III, it was estimated that the bicell sensor should have an accuracy in the order of tenth of microns (0.1 to 0.5 (μm)) in deflection measurement to achieve 0.2 (N) accuracy. This section evaluates the optical sensor in regards to this performance requirement. The analysis presented here is similar to the noise analysis of a bicell displacement sensor for atomic force microscopy presented by Barret and Quate [33]. Fig. 15 shows a schematic of the light that passes through the slit and emits the active elements in a bicell.

Figure 15. Schematics of a bicell photodiode; the yellow box shows the light beam passed through the slit

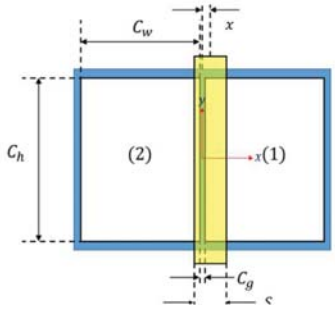

The projected light area on each active element is:

$$A_1 = C_h\left(\frac{S_w - C_g}{2} + x\right), A_2 = C_h\left(\frac{S_w - C_g}{2} - x\right) \quad (7)$$

where the symbols are defined in Fig. 15.

Assuming a uniform light intensity (I) of the IR LED in (w/m^2) and Responsivity of R in (A/w), the photocurrent generated at each cell is:

$$\begin{cases} I_1 = A_1 IR = IRC_h\left(\frac{S_w - C_g}{2} + x\right) \\ I_2 = A_2 IR = IRC_h\left(\frac{S_w - C_g}{2} - x\right) \end{cases}. \quad (8)$$

The sensitivity of the detector for small slit displacement (dx) is:

$$\frac{dI_1 - dI_2}{dx} = 2IRC_h. \quad (9)$$

With $I_0 = IRC_h\left(\frac{S_w - C_g}{2}\right)$, the uncertainty in the photocurrent generated within each cell is shot-noise limited:

$$\delta I_1 = \delta I_2 = \sqrt{2qI_0\Delta f} \quad (10)$$

where q is the electron charge, Δf is the measurement bandwidth. With the assumption that noises are uncorrelated, one can determine that:

$$\delta x = \delta(I_1 - I_2) \times \frac{dx}{d(I_1 - I_2)} = \sqrt{\frac{q(S_w - C_g)\Delta f}{2IRC_h}}. \quad (11)$$

In the current setup:

- $C_g = 0.1$ (mm)
- $S_w = 1$(mm)
- $I_1 + I_2 = IRC_h(S_w - C_g) = 182.75$ (μA).

Hence, IRC_h = 0.203 (A/m). The electronics have a bandwidth of 500 (Hz). Using (11), the uncertainty in displacement estimation (δx) due to the shot-noise limited photocurrents (δI) is 0.4 (nm); the optical transducer cannot resolve displacements smaller than 0.4 (nm) and this is a lower bound on the sensor capabilities. The estimated performance matches that of Barret and Quate [33], who claimed (6.1 (A^o_{rms})). The estimated uncertainty of 0.4 (nm) is orders of magnitude smaller than the required deflection estimation accuracy specified in Section III and mentioned in the beginning of this section.

VI. Conclusion and Future Work

The presented results show that it is feasible to use bicell photodiodes to estimate the forces applied at the tip of EndoWrist instruments. Although a bicell was used in this study, the results could be extended to quadcells as well.

The optical sensor showed linear response with no hysteresis behavior, it is inexpensive, and, in contrast to strain gauges, does not require special surface preparation, adhesives and coatings. No modification in the instrument structure was made which makes it adaptable to different EndoWrist instruments. The optical sensor could be quickly clamped on and off and is therefore easy to install. Because it is mounted onto the instrument shaft, the out of roundness, and other instrument fabrication tolerances along its entire length will have minor effect on the sensor readings. The sensor has no flexible component and is therefore very robust to overload up to the limits of the load-carrying structure (here instrument shaft). The low measurement noise allows for high bandwidth electronics and large gains in the signal conditioning circuit; therefore adjustable resolution and dynamic range. As an extreme example, we were able to increase the gain of the instrumentation amplifier and detect vibrations when people walk in the building.

The calibration results showed that although the sensor has a high bandwidth, the instrument structural dynamics between the force actuation point and the force measurement point significantly lower the measurements bandwidth. It may be possible to compensate for instrument dynamics to make use of the higher frequency response of the sensor in, for example, providing vibro-tactile feedback to the operator [37], [38].

In the next steps, we will be expanding the tested concept to a multi-axis force sensor design that could be used in a wide range of applications. Focused on RAMIS, we will be designing a low friction trocar and develop a calibration technique considering the varying boundary condition when the instrument penetrates into the trocar.

Acknowledgment

Amir Hossein Hadi Hosseinbabadi would like to appreciatively recognize scholarship support from the NSERC Canada Graduate Scholarships-Doctoral program. Professor Salcudean gratefully acknowledges infrastructure support from CFI and funding support from NSERC and the Charles Laszlo Chair in Biomedical Engineering. The authors would also like to acknowledge Intuitive Surgical for initial discussions (Dr. Simon DiMaio) and for providing EndoWrist instruments used in this study.

REFERENCES

[1] "www.intuitivesurgical.com/Company," *Intuitive Surgical Website*. .

[2] K. S. Shahzada, A. Yurkewich, R. Xu, and R. V Patel, "Sensorization of a surgical robotic instrument for force sensing," in *Proc. SPIE*, 2016, vol. 9702, p. 97020U–97020U–10.

[3] A. L. Trejos, R. V Patel, and M. D. Naish, "Force sensing and its application in minimally invasive surgery and therapy: A survey," *Proc. Inst. Mech. Eng. Part C J. Mech. Eng. Sci.*, vol. 224, no. 7, pp. 1435–1454, Jan. 2010.

[4] J. Jung, J. Lee, and K. Huh, "Robust contact force estimation for robot manipulators in three-dimensional space," *Proc. Inst. Mech. Eng. Part C J. Mech. Eng. Sci.*, vol. 220, no. 9, pp. 1317–1327, 2006.

[5] S. Katsura, W. Iida, and K. Ohnishi, "Medical mechatronics - An application to haptic forceps," *Annu. Rev. Control*, vol. 29, no. 2, pp. 237–245, Jan. 2005.

[6] A. Gupta, M. K. O'Malley, and V. Patoglu, "Disturbance Observer Based Closed Loop Force Control for Haptic Feedback," in *Volume 9: Mechanical Systems and Control, Parts A, B, and C*, 2007, pp. 1343–1349.

[7] A. J. Spiers, H. J. Thompson, and A. G. Pipe, "Investigating remote sensor placement for practical haptic sensing with EndoWrist surgical tools," in *IEEE World Haptics Conference, WHC 2015*, 2015, pp. 152–157.

[8] A. L. Trejos, R. V. Patel, M. D. Naish, and C. M. Schlachta, "Design of a sensorized instrument for skills assessment and training in minimally invasive surgery," in *Proceedings of the 2nd Biennial IEEE/RAS-EMBS International Conference on Biomedical Robotics and Biomechatronics, BioRob 2008*, 2008, pp. 965–970.

[9] J. Wee, R. J. Brooks, T. Looi, G. Azzie, J. Drake, and J. Ted Gerstle, "Force-Sensing Sleeve for Laparoscopic Surgery [1]," *J. Med. Device.*, vol. 10, no. 3, p. 030946, Aug. 2016.

[10] D. Jones, A. Lewis, and G. S. Fischer, "Development of a standalone surgical haptic arm," in *Proceedings of the Annual International Conference of the IEEE Engineering in Medicine and Biology Society, EMBS*, 2011, pp. 2136–2139.

[11] H. Mayer, F. Gomez, D. Wierstra, I. Nagy, A. Knoll, and J. Schmidhuber, "A system for robotic heart surgery that learns to tie knots using recurrent neural networks," *IEEE Int. Conf. Intell. Robot. Syst.*, vol. 22, no. 13–14, pp. 543–548, Jan. 2006.

[12] A. L. Trejos, A. C. Lyle, A. Escoto, M. D. Naish, and R. V. Patel, "Force/position-based modular system for minimally invasive surgery," in *Proceedings - IEEE International Conference on Robotics and Automation*, 2010, pp. 3660–3665.

[13] N. Zemiti, G. Morel, T. Ortmaier, and N. Bonnet, "Mechatronic design of a new robot for force control in minimally invasive surgery," *IEEE/ASME Trans. Mechatronics*, vol. 12, no. 2, pp. 143–153, Apr. 2007.

[14] S. Perreault, A. Talasaz, A. L. Trejos, C. D. W. Ward, R. V. Patel, and B. Kiaii, "A 7-DOF haptics-enabled teleoperated robotic system: Kinematic modeling and experimental verification," in *2010 3rd IEEE RAS and EMBS International Conference on Biomedical Robotics and Biomechatronics, BioRob 2010*, 2010, pp. 906–911.

[15] U. Seibold, B. Kuebler, and G. Hirzinger, "Prototypic force feedback instrument for minimally invasive robotic surgery," in *Medical Robotics*, vol. 44, no. Section 5, INTECH, 2007, pp. 377–400.

[16] J. Jiang, L. Xie, and H. Yu, "A 6-Axis Sensor for Minimally Invasive Robotic Surgery," in *International Conference on Intelligent Robotics and Applications*, 2013, pp. 429–435.

[17] G. S. Fischer *et al.*, "Ischemia and force sensing surgical instruments for augmenting available surgeon information," in *Proceedings of the First IEEE/RAS-EMBS International Conference on Biomedical Robotics and Biomechatronics, (BioRob)*, 2006, pp. 1030–1035.

[18] S. Shimachi, Y. Hakozaki, T. Tada, and Y. Fujiwara, "Measurement of force acting on surgical instrument for force-feedback to master robot console," *Int. Congr. Ser.*, vol. 1256, no. C, pp. 538–546, 2003.

[19] S. Shimachi, Y. Fujiwara, and Y. Hakozaki, "New sensing method of force acting on instrument for laparoscopic robot surgery," *Int. Congr. Ser.*, vol. 1268, no. C, pp. 775–780, 2004.

[20] H. Wang, B. Kang, and D. Y. Lee, "Design of a slave arm of a surgical robot system to estimate the contact force at the tip of the employed instruments," *Adv. Robot.*, vol. 28, no. 19, pp. 1305–1320, Oct. 2014.

[21] A. L. Trejos, A. Escoto, D. Hughes, M. D. Naish, and R. V. Patel, "A sterilizable force-sensing instrument for laparoscopic surgery," in *Proceedings of the IEEE RAS and EMBS International Conference on Biomedical Robotics and Biomechatronics*, 2014, pp. 157–162.

[22] U. Kim, D. H. Lee, W. J. Yoon, B. Hannaford, and H. R. Choi, "Force Sensor Integrated Surgical Forceps for Minimally Invasive Robotic Surgery," *IEEE Trans. Robot.*, vol. 31, no. 5, pp. 1214–1224, Oct. 2015.

[23] G. Tholey, A. Pillarisetti, W. Green, and J. P. Desai, "Design, Development, and Testing of an Automated Laparoscopic Grasper with 3-D Force Measurement Capability," in *Lecture Notes in Computer Science*, 2004, vol. 3078, no. June 2016, pp. 38–48.

[24] K. Tadano and K. Kawashima, "Development of a Master–Slave System with Force-Sensing Abilities using Pneumatic Actuators for Laparoscopic Surgery," *Adv. Robot.*, vol. 24, no. 12, pp. 1763–1783, 2010.

[25] P. Valdastri *et al.*, "Integration of a miniaturised triaxial force sensor in a minimally invasive surgical tool," *IEEE Trans. Biomed. Eng.*, vol. 53, no. 11, pp. 2397–2400, 2006.

[26] M. Lazeroms, "Optical fibre force sensor for minimal-invasive-surgery grasping instruments," in *18th Annual International Conference of the IEEE Engineering in Medicine and Biology Society*, 1996, vol. 1, pp. 234–235.

[27] J. Peirs *et al.*, "A micro optical force sensor for force feedback during minimally invasive robotic surgery," *Sensors Actuators, A Phys.*, vol. 115, no. 2–3 SPEC. ISS., pp. 447–455, 2004.

[28] M. S. Müller, L. Hoffmann, T. C. Buck, and A. W. Koch, "Fiber bragg grating-based force-torque sensor with six degrees of freedom," *Int. J. Optomechatronics*, vol. 3, no. 3, pp. 201–214, 2009.

[29] R. Haslinger, P. Leyendecker, and U. Seibold, "A fiberoptic force-torque-sensor for minimally invasive robotic surgery," in *Proceedings - IEEE International Conference on Robotics and Automation*, 2013, pp. 4390–4395.

[30] H. Song, H. Kim, J. Jeong, and J. Lee, "Development of FBG sensor system for force-feedback in minimally invasive robotic surgery," in *Proceedings of the International Conference on Sensing Technology, ICST*, 2011, pp. 16–20.

[31] P. Puangmali, H. Liu, L. D. Seneviratne, P. Dasgupta, and K. Althoefer, "Miniature 3-axis distal force sensor for minimally invasive surgical palpation," *IEEE/ASME Trans. Mechatronics*, vol. 17, no. 4, pp. 646–656, Aug. 2012.

[32] G. A. Fontanelli, L. Buonocore, F. Ficuciello, L. Villani, and B. Siciliano, "A novel force sensing integrated into the trocar for minimally invasive robotic surgery," *IEEE/RSJ Int. Conf. Intell. Robot. Syst.*, 2017.

[33] R. C. Barrett and C. F. Quate, "Optical scan-correction system applied to atomic force microscopy," *Rev. Sci. Instrum.*, vol. 62, no. 6, pp. 1393–1399, 1991.

[34] R. A. Beasley and R. D. Howe, "Increasing Accuracy in Image-Guided Robotic Surgery Through Tip Tracking and Model-Based Flexion Correction," *IEEE Trans. Robot.*, vol. 25, no. 2, pp. 292–302, Apr. 2009.

[35] F. P. Beer, E. R. J. Johnston, J. T. DeWolf, and D. F. Mazurek, *Mechanics of Materials*, 7th ed. New York: McGraw-Hill Higher Education, 2009, 1967.

[36] W. Thomson and M. D. Dahleh, *Thomson et al - 1998 - Theory of Vibration with Applications*, 5th ed. Prentice-Hall, Inc., 1998.

[37] K. Bark *et al.*, "In Vivo Validation of VerroTouch: Tactile Feedback of Tool Vibrations for Robotic Surgery," *Surg Endosc.*, vol. 27, pp. 656–664, 2013.

[38] K. J. Kuchenbecker *et al.*, "VerroTouch: High-frequency acceleration feedback for telerobotic surgery," in *EuroHaptics 2010*, vol. 6191 LNCS, no. PART 1, Springer, Berlin, Heidelberg, 2010, pp. 189–196.